

Modeling the Capacitive Nonlinearity in Thin-Film BST Varactors

David R. Chase, *Member, IEEE*, Lee-Yin Chen, *Member, IEEE*, and Robert A. York, *Senior Member, IEEE*

Abstract—A simple closed-form expression for the dielectric nonlinearity in thin-film high-permittivity barium strontium titanate (BST) devices is obtained from a third-order power-series expansion for the field-polarization relation. The expression is parameterized in terms of easily measurable quantities of zero-field capacitance and tuning ratio, and compares favorably with data on several representative BST compositions and device sizes. The temperature dependence of the capacitors is treated using a simple linear temperature coefficient in the zero-field capacitance that also compares favorably with experimental data on BST capacitors. The influence of interfacial (“dead” layer), fringing, and parasitic shunt capacitance on the experimental C - V curves is discussed. The results are potentially useful for circuit and electromagnetic simulation.

Index Terms—Ferroelectrics, integrated passives, nonlinear dielectrics, varactors.

I. INTRODUCTION

HIGH-PERMITTIVITY thin-film dielectrics may exhibit a strong field dependence in the dielectric constant that can be exploited for voltage-variable capacitors in RF circuits. Thin-film barium strontium titanate (BST) and bismuth zinc niobate (BZN) are examples of materials that have been investigated for RF applications [1]–[7]. For device and circuit design, it is desirable to have a simple analytic expression for the capacitance–voltage nonlinearity. This paper derives a convenient closed-form expression for the field or voltage dependence of BST devices in the paraelectric regime as a function of the geometry, film thickness, and temperature. The expression is parameterized in terms of the easily measurable quantities of zero-field capacitance, and tuning ratio at a given voltage, most notably the “2 : 1 voltage” (or field). This expression is shown to compare favorably against measured data. We also discuss the effects of the so-called “dead” layer, fringing capacitance, and other parasitics on the measured C - V curves, along with the temperature dependence of capacitance.

Manuscript received March 3, 2005; revised May 4, 2005. This work was supported by the Army Research Office under the Multifunctional Adaptive Radar and Radio Sensors Multiuniversity Research Initiative Project DAAD19-01-1-0496, and by the Defense Advanced Research Projects Agency under the Center for Nanoscience Innovation for Defense Grant DMEA90-02-2-0215.

D. R. Chase is with Vareda Inc., Goleta, CA 93117 USA (e-mail: dchase@vareda.com).

L.-Y. Chen is with Agile Materials and Technologies Inc., Goleta, CA 93117 USA (e-mail: chen@agilematerials.com).

R. A. York is with the Electrical and Computer Engineering Department, University of California at Santa Barbara, Santa Barbara, CA 93106 USA (e-mail: rayork@ece.ucsb.edu).

Digital Object Identifier 10.1109/TMTT.2005.855141

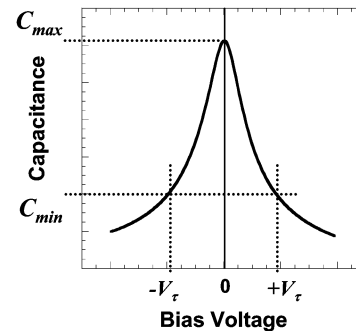


Fig. 1. Tunability curve and definitions for max and min capacitance.

II. IDEAL PARAELECTRIC NONLINEARITY

Varactors made from high-permittivity materials should have symmetrical small-signal C - V characteristics, as shown in Fig. 1. The peak capacitance at zero applied field is C_{\max} . As the applied dc field increases, the small-signal capacitance dQ/dV decreases monotonically. At some voltage V_{τ} the capacitance is reduced to C_{\min} ; we define the *tunability* as the ratio of maximum-to-minimum capacitance at this voltage as follows:

$$\tau = \frac{C_{\max}}{C_{\min}}. \quad (1)$$

The tunability thus defined is dependent on the choice of V_{τ} . In this analysis V_{τ} can be chosen arbitrarily, but it is shown later that the “2 : 1” voltage V_2 is an obvious choice.

Vendik and Zubko [8] have presented a field- and temperature-dependent permittivity model for ferroelectrics based on a detailed consideration of the underlying physics. As a starting point toward a simpler empirical model we assume a power-series expansion for the field-polarization relation of the form [9], [10]

$$E = \alpha_1(T)D + \alpha_3 D^3 + \dots \quad (2)$$

where $\alpha_1(T)$ is the inverse of the zero-bias permittivity (temperature dependent) and α_3 describes the nonlinearity of the material. In the context of ferroelectric films, (2) is called the Landau–Devonshire–Ginzburg (LDG) model.

For an ideal capacitor (no interfacial layers or space charge) we can assume that the E -field and flux density D are uniform throughout the film, and relate to the external applied voltage and charge through

$$E = \frac{V}{d} \quad D = \frac{Q}{A} \quad (3)$$

where d is the capacitor thickness and A is the area. This transforms (2) into

$$V = \frac{\alpha_1 d}{A} Q + \frac{\alpha_3 d}{A^3} Q^3 \quad (4)$$

The device capacitance is defined by

$$C(V) = \frac{dQ}{dV} \quad (5)$$

from which the zero-field capacitance is found as

$$C_{\max} \equiv \left. \frac{dQ}{dV} \right|_{V=Q=0} = \frac{A}{\alpha_1 d} = \frac{\varepsilon_b A}{d} \quad (6)$$

and, hence, the apparent permittivity at zero field is just $\varepsilon_b = 1/\alpha_1$ and temperature dependent. It is helpful to introduce the normalized variables

$$v = \frac{V}{V_\tau} \quad q = \frac{Q}{C_{\max} V_\tau} \quad (7)$$

so that the governing equation becomes

$$v = q + bq^3 \quad (8)$$

where b is just an empirical constant that we will relate to the tunability parameter τ . Using (8), the normalized capacitance is

$$c(v) \equiv \frac{C(V)}{C_{\max}} = \frac{dq}{dv} = \frac{1}{1 + 3bq^2} \quad (9)$$

where q is an implicit function of voltage through (8). If we define the normalized charge at $v = 1$ as q_τ , then (8) and (9) require that

$$q_\tau (1 + bq_\tau^2) = 1 \quad \tau = 1 + 3bq_\tau^2. \quad (10)$$

These can be solved simultaneously to give

$$b = \frac{(\tau - 1)(\tau + 2)^2}{3^3}. \quad (11)$$

As shown in [10], (9) can be made an explicit function of voltage by inverting (8) to give

$$q(v) = \frac{\zeta(v)}{18^{1/3} \sqrt{b}} - \frac{\left(\frac{2}{3}\right)^{1/3}}{\sqrt{b} \zeta(v)} \quad (12)$$

where

$$\zeta(v) = \left(9v\sqrt{b} + \sqrt{12 + 81bv^2}\right)^{1/3}.$$

This result is exact, but cumbersome. A simpler equivalent can be obtained using the substitution

$$q = \beta \sinh \theta. \quad (13)$$

Inserting this into (8) and rearranging gives

$$\sinh^3 \theta + \frac{1}{b\beta^2} \sinh \theta - \frac{v}{b\beta^3} = 0. \quad (14)$$

Note the similarity to the hyperbolic identity

$$\sinh^3 \theta + \frac{3}{4} \sinh \theta - \frac{1}{4} \sinh 3\theta = 0. \quad (15)$$

Comparing terms in (14) and (15) gives

$$\frac{1}{b\beta^2} = \frac{3}{4} \quad \frac{v}{b\beta^3} = \frac{1}{4} \sinh 3\theta. \quad (16)$$

Equation (13) and (16) can now be combined to give the required charge–voltage and, hence, $c(v)$ relationship

$$c(v) = \frac{dq}{dv} = \frac{\partial q}{\partial \theta} \frac{\partial \theta}{\partial v} = \frac{1}{2 \cosh 2\theta - 1}. \quad (17)$$

where

$$\theta = \frac{1}{3} \sinh^{-1} \left[\frac{v}{2} \sqrt{3^3 b} \right]$$

Replacing the normalized variables with physically meaningful quantities gives the desired end result

$$C(V) = \frac{C_{\max}}{2 \cosh \left[\frac{2}{3} \sinh^{-1} \left(\frac{2V}{V_2} \right) \right] - 1}. \quad (18)$$

This is the central result of this paper. Note we have introduced a new variable V_2 that is defined as

$$V_2 = \frac{4V_\tau}{(\tau + 2) \sqrt{\tau - 1}}. \quad (19)$$

This is the “2 : 1” voltage at which $C(V_2) = C_{\max}/2$, an easily measured quantity. Experimentally there are only two parameters that define the ideal $C(V)$ curve: C_{\max} and V_2 . Once we know V_2 for a given device, (19) can also be used to determine the voltage required to achieve a desired tunability.

For completeness we note that the original LDG expansion (2) has now been successfully inverted as

$$D(E) = \frac{3}{2} \varepsilon_b E_2 \sinh \left[\frac{1}{3} \sinh^{-1} \left(\frac{2E}{E_2} \right) \right] \quad (20)$$

where $E_2 = V_2/d$ is the field at which the permittivity changes is reduced by a factor of 2, and $\varepsilon_b = 1/\alpha_1$ is the zero-bias permittivity. This is a potentially useful result for electromagnetic (EM) simulators.

III. ASYMPTOTIC APPROXIMATIONS

Before comparing the analytic result with the experiment it is worthwhile to explore the behavior of (18) at the extremes of

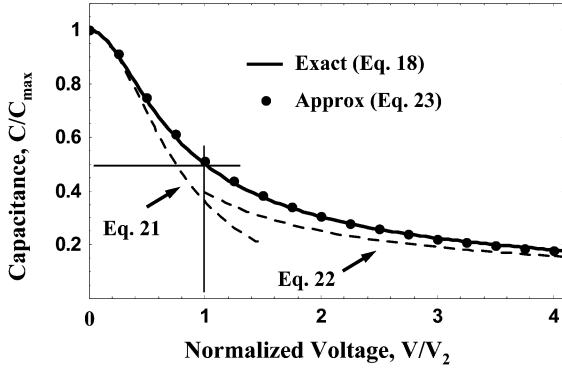


Fig. 2. Comparison of exact and approximate $C(V)$ relations.

applied field. The asymptotic behavior of (18) in the low-field limit $V \ll V_2$ is then

$$C(V) \approx \frac{C_{\max}}{1 + \left(\frac{4V}{3V_2}\right)^2} \text{ for } V \ll V_2. \quad (21)$$

At the high-field extreme where $V \gg V_2$, the asymptotic behavior is given by

$$C(V) \approx \frac{C_{\max}}{\left(\frac{4V}{V_2}\right)^{2/3}} \text{ for } V \gg V_2. \quad (22)$$

An empirical expression that gives a reasonably good match to these low- and high-field asymptotes is given by

$$C(V) = \frac{C_{\max}}{\left[1 + \left(\frac{2V}{V_2}\right)^2\right]^\gamma} \quad \gamma = 0.417. \quad (23)$$

This expression is similar to that used in [6], and is plotted in Fig. 2 with the exact theoretical C - V curve (18), along with the asymptotic behavior in (21) and (22).

IV. COMPARISON WITH LARGE-CAPACITOR DATA

The ideal $C(V)$ curve (18) compares favorably with experimental data, as shown in Fig. 3. For this comparison, a relatively large-area device ($2000 \mu\text{m}^2$) was chosen to minimize the peripheral parasitics discussed later. The BST is a high-tunability sputtered $\text{Ba}_{0.5}\text{Sr}_{0.5}\text{TiO}_3$ composition, 140-nm thick, with Pt electrodes. The BST growth conditions and device processing are described in more detail in [11]. This data was measured on an RF probe station with 50- μm -pitch APC40 ground-signal-ground (GSG) probes using an Agilent 4294 impedance analyzer. The CV curves were taken at 1 MHz with a 200-mV ac signal amplitude.

Certain growth or processing conditions can result in space-charge buildup near one of the electrodes. This can also happen after long-term exposure to high fields as a result of the migration of charged defects such as oxygen vacancies. In each case, the space charge produces a built-in field, which shifts the peak of the $C(V)$ curve to a new voltage V_{peak} . Although this is typically an indicator of a poor quality or damaged film, the effect can be modeled if desired by inserting $V - V_{\text{peak}}$ into

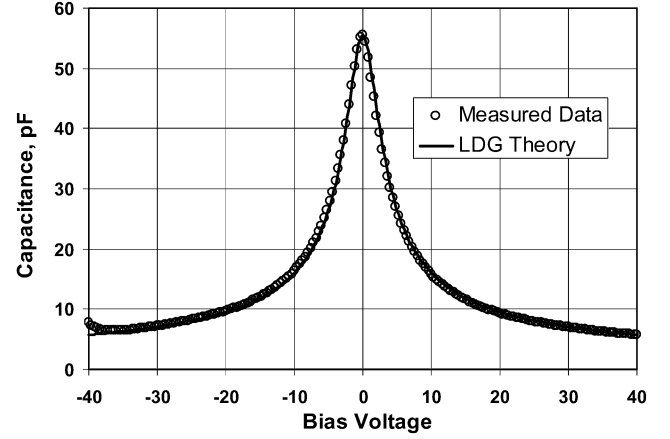


Fig. 3. Comparison of the theoretical $C(V)$ relation (18) with measured data on a high-tunability sputtered BST device.

(18) in place of the voltage V . No peak shift was required to model the data in Fig. 3.

V. SMALL CAPACITORS AND FRINGING EFFECTS

Dielectric varactors have a high capacitance density, up to 100 times that of conventional integrated capacitors using SiO_2 or SiN dielectrics. The typical electrode areas are, therefore, much smaller by comparison, and the periphery-to-area ratios are much higher for a given total capacitance.

Experimentally, we observe that smaller capacitors have a reduced tunability compared with larger devices on the same wafer. This appears to be well modeled by a *nontunable* “fringing” capacitance in parallel with the tunable device. As the device size is reduced, this contribution represents an increasing fraction of the overall capacitance, and the tuning curves are observed to level off prematurely. Our data is consistent with a fringing capacitance of the form

$$C_f = \kappa \frac{P}{d} \quad (24)$$

so that

$$C(V) = \frac{C_{\max} - C_f}{2 \cosh \left[\frac{2}{3} \sinh^{-1} \left(\frac{2V}{V_2} \right) \right] - 1} + C_f \quad (25)$$

where P is the device periphery, and κ is a constant with the dimensions of capacitance that appears to be independent of field or material thickness d .

Fig. 4 shows the tuning curves for several small-area devices and a comparison to the theoretical model with and without the fringing correction. The devices were made using sputtered 30/70 BST with Pt electrodes. In contrast to Fig. 3, this data was extracted from broad-band on-wafer RF data measured from 50 MHz to 20 GHz on an Agilent E8364A PNA-series network analyzer. The device capacitance was determined by first deembedding the probe pad parasitics, and fitting the resulting data to an equivalent circuit model to remove the effects of residual series inductance. The dashed curves in Fig. 4 were generated from (18) using $V_2 = 13$ V, a value determined experimentally from larger area devices on the same wafer. The solid curves

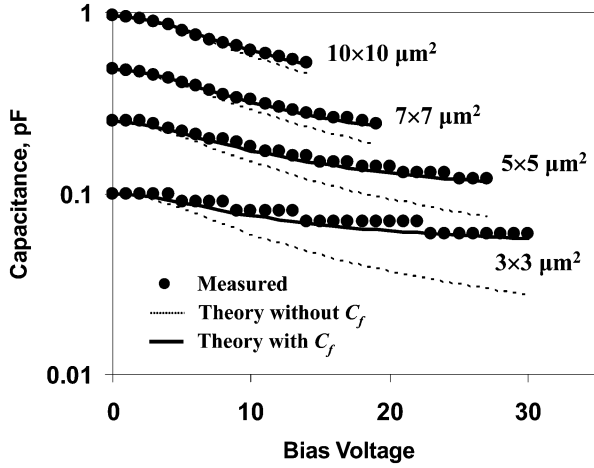


Fig. 4. Comparison of the theoretical $C(V)$ relation with measured RF data on small-area devices. The dashed line is the ideal model (18) using $V_2 = 13$ V. The solid line is (25) with the fringing correction added. Note the data resolution of 0.01 pF apparent in the measurement for the 3×3 device.

were generated from (25) using $\kappa = 0.6$ fF and a measured film thickness of $d = 210$ nm. The data is shown on a log scale in capacitance for clarity.

Note that the thickness dependence proposed in (24) is somewhat different than a conventional fringing model (e.g., [16]) in which κ should scale almost linearly with d and, hence, a fringing capacitance that is roughly independent of thickness. Although the data in Fig. 4 is at a fixed film thickness, thickness-dependent data is presented later (Section VI) that is also consistent with the thickness dependence of (24). Furthermore, numerical modeling on idealized structures suggests that κ should be field dependent and, hence, C_f should minimally impact the tunability, but the data does not support this conclusion.

It should be noted that the small-area devices of Fig. 4 required a dielectric crossover to form the electrical contact to the top electrode and this introduces a parallel capacitance that adds to C_f ; care was taken to minimize this contribution through device design, estimated to be <5 fF for the devices described here. Also, at very high fields the leakage currents in thin-film capacitors can be substantial and cause an apparent increase in capacitance density because the injected charge lowers the internal field; care was taken to insure that this was not a factor in these measurements.

VI. INFLUENCE OF THE INTERFACIAL CAPACITANCE

Permittivity values extracted from measurements on thin-film capacitors can show a strong thickness dependence. This has previously been explained by the presence of a nontunable interfacial capacitance [9], [10]. There is no general agreement yet on the exact origin of this capacitance, but two possible candidates are, which are: 1) an effective interfacial capacitance due to field penetration into the electrodes [12] or 2) an interfacial capacitance associated with near-surface charge traps [13]. These effects should also be present in any thin-film capacitor, but for low-permittivity materials they would ordinarily have a negligible impact because the interfacial capacitance is so large, typically on the order of $30\text{--}60$ fF/ μm^2 . For high-permittivity

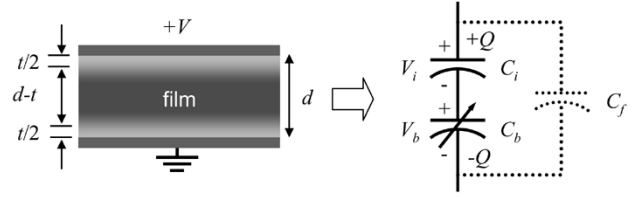


Fig. 5. Interfacial capacitance in thin-film varactors contributes a nontunable “dead layer” that can reduce the overall tunability of the device.

materials, the bulk and interfacial capacitance densities may be comparable in value, particularly for very thin materials that are desired for low control voltages.

Experimental data suggests that the interfacial capacitance is not tunable and hence is sometimes referred to as a “dead” layer, in which case the composite effect would be modeled by a fixed-value capacitance in series with the bulk nonlinear material [9].

The applied voltage is dropped partly across the dead layer and partly across the bulk layer. With reference to Fig. 5, the two interfacial dead layers are collectively described by a linear charge–voltage relationship

$$V_i = \frac{Q}{C_i} \quad C_i = \frac{\epsilon_i A}{t} \quad (26)$$

and the interfacial capacitance density ϵ_i/t can be determined from a series of devices of varying film thickness [9], and this also yields an estimate for the bulk zero-bias permittivity ϵ_b . The bulk is described by the nonlinear relationship (4)

$$V_b = \frac{Q}{C_{b,\max}} + KQ^3 \quad (27)$$

where

$$\frac{1}{C_{b,\max}} = \frac{\alpha_1(d-t)}{A} \approx \frac{d}{\epsilon_b A} \quad K = \frac{\alpha_3(d-t)}{A^3} \approx \frac{\alpha_3 d}{A^3} \quad (28)$$

The total voltage across the device is then

$$V = Q \left(\frac{1}{C_i} + \frac{1}{C_{b,\max}} \right) + KQ^3 \quad (29)$$

This relationship can be put in the form of (8) if we define

$$\frac{1}{C_{\max}} = \left(\frac{1}{C_i} + \frac{1}{C_{b,\max}} \right) \quad (30)$$

and

$$b = \alpha_3 d \left(\frac{C_{\max}}{A} \right)^3 V_\tau^2 \quad (31)$$

Thus we expect the same functional form for the $C(V)$ relationship as the ideal case (18), but with thickness-dependent parameters $C_{\max}(d)$ and $V_2(d)$.

For device optimization, it is helpful to make the thickness dependence more explicit, especially with regards to the tradeoffs between control voltage and power handling or linearity. Once the interfacial capacitance density is determined, we need only measure the maximum capacitance and 2:1 voltage at some

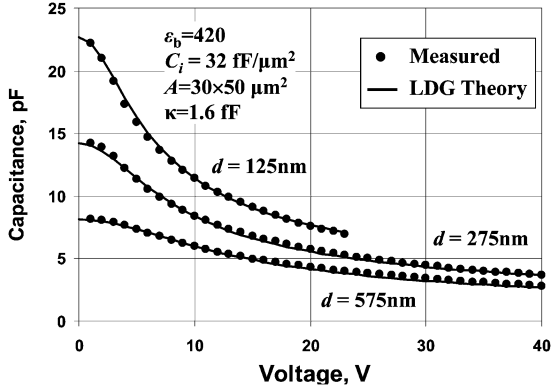


Fig. 6. Measured data on devices of varying film thickness and comparison with the thickness-dependent model using the parameters shown.

nominal material thickness d_0 . Using (30) and (31), the general thickness-dependent tuning parameters become

$$C_{\max}(d) = \frac{1}{\frac{1}{C_i} + \frac{d}{d_0} \left[\frac{1}{C_{\max}(d_0)} - \frac{1}{C_i} \right]} \quad (32)$$

and

$$\frac{V_2(d)}{V_2(d_0)} = \sqrt{\frac{d_0 C_{\max}^3(d_0)}{d C_{\max}^3(d)}}. \quad (33)$$

$C(V, d)$ is then uniquely determined for any film thickness by the specification of C_i , $C_{\max}(d_0)$, and $V_2(d_0)$.

Fig. 6 shows the data for three devices of identical electrode area, processed from three different thicknesses of low-barium BST with Pt electrodes. These films were part of a more extensive thickness series that was used to determine an interfacial capacitance density of ~ 32 fF/ μm^2 and a bulk permittivity of $\varepsilon_b = 420$. The data was extracted from broad-band RF data taken on a network analyzer, as described earlier. Using these parameters, and using the 575-nm material as the reference, the theoretical curves for each device were generated from (18), (32), and (33). A peripheral contribution was added according to (24) using $\kappa = 1.6$ fF. Excellent agreement is observed using the dead-layer model for the thickness dependence.

In practice, the long-term reliability of dielectric varactors (and thin-film capacitors in general) has been shown to depend critically on the maximum bias field $E = V/d$ (see [14] and [15] for an example). Fig. 7 shows the tunability at a fixed field versus film thickness, using (32) and (33), along with data from Fig. 6.

VII. TEMPERATURE DEPENDENCE

The temperature dependence of BST thin films has been formally addressed in [9], [17], and [18]. Stress in the films due to a thermal-expansion mismatch with the substrate tends to greatly reduce the temperature sensitivity of the permittivity as compared with bulk materials. An applied field reduces the sensitivity further. The thermal sensitivity is thickness dependent due to the combination of stress and the dead-layer effect. Over the range of temperatures normally encountered in practical applications (from -40 °C to $+100$ °C), experiments show that thin

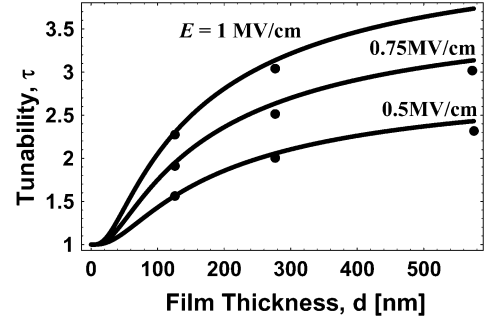


Fig. 7. Predicted tunability versus thickness for a constant applied field using the parameters described in Fig. 6. The dots are measurements.

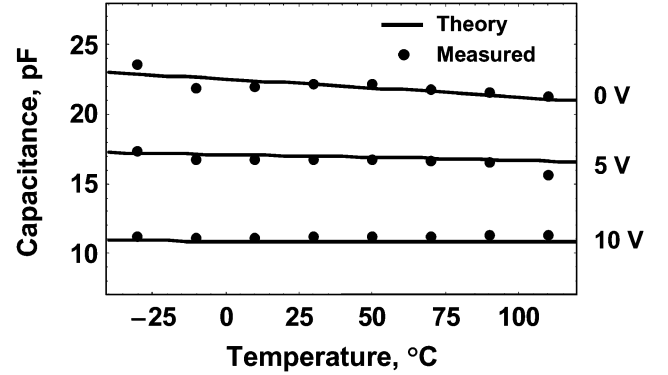


Fig. 8. Measured data on devices of varying film thickness and comparison with the thickness-dependent model using the parameters shown.

films are reasonably well modeled by a linear temperature coefficient for the low-field permittivity such that

$$\varepsilon_b(T) \approx \varepsilon_{b0} [1 - \beta(T - T_0)] \quad (34)$$

where β is the temperature coefficient of capacitance (TCC) at zero bias, usually specified in ppm/°C. Typical numbers for BST thin films range from 500 to 1000 ppm/°C, somewhat better than an X7R capacitor material.

Inserting (34) into (28) leaves us with a complete model that describes the thickness, size, and temperature dependence of the device. Fig. 8 shows the calculated temperature-dependent curves for a BST film similar to that in Fig. 6, along with measured data, showing good agreement with the simple model. Note that the zero-bias case always has the strongest temperature dependence, whereas the biased device typically shows a very small TCC.

VIII. CONCLUSION

We have derived a simple closed-form analytical expression for the $C(V)$ relation in thin-film dielectric varactors, and presented a complete model describing the observed thickness, size, and temperature dependence for such devices. The model compares favorably with measurements. As the electrode area decreases, departures from the ideal are observed as peripheral parasitics become important. The peripheral contribution to capacitance needs to be better understood. Future research will also focus on understanding the large-signal implications of the $C(V)$ nonlinearity for understanding harmonic distortion and

intermodulation distortion (IMD) in circuits using dielectrics varactors.

ACKNOWLEDGMENT

The authors wish to thank Ms. N. Pervez, University of California at Santa Barbara (UCSB), for contributing the large-area 50/50 BST device data. The authors also thank M. Fink and R. Forse, both with Agile Materials and Technologies, Goleta, CA, for the C - V measurements of 30/70 BST capacitors, and Dr. C. Elsass and Dr. T. Taylor, also with Agile Materials and Technologies, for the thickness-series data.

REFERENCES

- [1] R. A. York, A. Nagra, E. Erker, T. Taylor, P. Periaswamy, J. Speck, S. Streiffer, and O. Auciello, "Microwave integrated circuits using thin-film BST," in *Proc. 12th Int. Applications of Ferroelectrics Symp.*, vol. 1, Jul. 2000, pp. 195–200.
- [2] A. Tombak, J.-P. Maria, F. T. Ayguavives, J. Zhang, G. T. Stauff, A. I. Kingon, and A. Mortazawi, "Tunable barium strontium titanate thin film capacitors for RF and microwave applications," *IEEE Microw. Wireless Compon. Lett.*, vol. 12, no. 1, pp. 3–5, Jan. 2002.
- [3] B. Acikel, T. R. Taylor, P. J. Hansen, J. S. Speck, and R. A. York, "A new high performance phase shifter using $Ba_xSr_{1-x}TiO_3$ thin films," *IEEE Microw. Wireless Compon. Lett.*, vol. 12, no. 7, pp. 237–239, Jul. 2002.
- [4] A. Tombak, J.-P. Maria, F. T. Ayguavives, J. Zhang, G. T. Stauff, A. I. Kingon, and A. Mortazawi, "Voltage-controlled RF filters employing thin-film barium–strontium–titanate tunable capacitors," *IEEE Trans. Microw. Theory Tech.*, vol. 51, no. 2, pp. 462–467, Feb. 2003.
- [5] A. Vorobiev, P. Rundqvist, K. Khamchane, and S. Gevorgian, "Silicon substrate integrated high Q -factor parallel-plate ferroelectric varactors for microwave/millimeterwave applications," *Appl. Phys. Lett.*, vol. 83, pp. 3144–3144, 2003.
- [6] L.-Y. Chen, R. Forse, D. Chase, and R. York, "Analog tunable matching network using integrated thin-film BST capacitors," in *IEEE MTT-S Int. Microwave Symp. Dig.*, vol. 1, Jun. 2004, pp. 261–264.
- [7] J. Lu and S. Stemmer, "Low-loss, tunable bismuth zinc niobate films deposited by RF magnetron sputtering," *Appl. Phys. Lett.*, vol. 83, pp. 2411–2411, 2003.
- [8] O. G. Vendik and S. P. Zubko, "Modeling the dielectric response of incipient ferroelectrics," *J. Appl. Phys.*, vol. 82, pp. 4475–4483, Nov. 1987.
- [9] C. Basceri, "The dielectric response as a function of temperature and film thickness of fiber-textured $(Ba,Sr)TiO_3$ thin films grown by chemical vapor deposition," *J. Appl. Phys.*, vol. 82, pp. 2497–2504, Sep. 1987.
- [10] J. D. Baniecki *et al.*, "Hydrogen induced tunnel emission in $pt/(Ba_xSr_{1-x})Ti_{1+y}O_{3+z}/pt$ thin film capacitors," *J. Appl. Phys.*, vol. 89, no. 5, pp. 2873–2885, Mar. 2001.
- [11] N. K. Pervez, P. J. Hansen, and R. A. York, "High tunability barium strontium titanate thin films for RF circuit applications," *Appl. Phys. Lett.*, vol. 85, pp. 4451–4451, 2004.
- [12] C. T. Black and J. J. Welser, "Electric-Field penetration into metals: Consequences for high-dielectric-constant capacitors," *IEEE Trans. Electron Devices*, vol. 46, no. 4, pp. 776–780, Apr. 1999.
- [13] H. Rohdin, N. Moll, A. M. Bratkovsky, and C.-Y. Su, "Dispersion and tunneling analysis of the interfacial gate resistance in Schottky barriers," *Phys. Rev. B, Condens. Matter*, vol. 59, pp. 13 102–13 113, May 1999.
- [14] T. Horikawa, T. Kawahara, M. Yamamuka, and K. Ono, "Degradation in $(Ba,Sr)TiO_3$ thin films under DC and dynamic stress conditions," in *35th Annu. Proc. IEEE Int. Reliability Physics Symp.*, 1997, pp. 82–89.
- [15] M. S. Tsai, S. C. Sun, and T. Y. Tseng, "Effect of oxygen to argon ratio on properties of $(Ba,Sr)TiO_3$ thin films prepared by radio-frequency magnetron sputtering," *J. Appl. Phys.*, vol. 82, pp. 3482–3487, Oct. 1997.
- [16] R. Plonsey and R. E. Collin, *Principles and Applications of Electromagnetic Fields*. New York: McGraw-Hill, 1961, pp. 162–162.
- [17] S. K. Streiffer *et al.*, "Ferroelectricity in thin films: The dielectric response of fiber-textured $(Ba_xSr_{1-x})Ti_{1+y}O_{3+z}$ thin films grown by chemical vapor deposition," *J. Appl. Phys.*, vol. 86, pp. 4565–4575, Oct. 1999.
- [18] T. R. Taylor, P. J. Hansen, B. Acikel, N. Pervez, R. A. York, S. K. Streiffer, and J. S. Speck, "Impact of thermal strain on the dielectric constant of sputtered barium strontium titanate thin films," *Appl. Phys. Lett.*, vol. 80, pp. 1978–1978, 2002.



David R. Chase (S'80–M'84) received the B.S. (with highest honors) and M.S. degrees in electrical engineering from the University of California at Santa Barbara (UCSB), in 1984 and 1988, respectively.

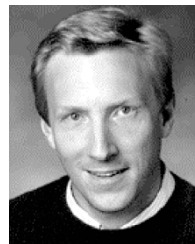
He is currently President of Vareda Engineering Inc., Goleta, CA, where he and his group are involved with the research and development and production of advanced communications and controller products for government and commercial customers. Prior to Vareda Engineering Inc., he held senior positions with Agile Materials and Technologies

Inc., Superconductor Technologies Inc., and Network Equipment Technologies, where he and his groups developed wireless and wire-line communications systems, subsystems, and components. His current research interests are the development of nonlinear adaptive signal processing techniques for wireless applications.



Lee-Yin (Vicki) Chen (M'01) received the B.S. degree in electrical engineering from National Taiwan University, Taipei, Taiwan, R.O.C., in 1997, and the M.S. and Ph.D. degrees in electrical and computer engineering from the University of California at Santa Barbara (UCSB), in 1999 and 2003, respectively.

She is currently with Agile Materials and Technologies Inc., Goleta, CA, where she is involved in the research and development effort and the RF and microwave circuit design for various applications. Her research has included microwave power-amplifier design and high-efficiency spatial power-combining techniques.



Robert A. York (S'85–M'89–SM'99) received the B.S. degree in electrical engineering from the University of New Hampshire, Durham, in 1987, and the M.S. and Ph.D. degrees in electrical engineering from Cornell University, Ithaca, NY, in 1989 and 1991, respectively.

He is currently a Professor of electrical and computer engineering with the University of California at Santa Barbara (UCSB), where his group is currently involved with the design and fabrication of novel microwave and millimeter-wave circuits, high-power microwave and millimeter-wave amplifiers using spatial combining and wide-bandgap semiconductor devices, and application of ferroelectric materials to microwave and millimeter-wave circuits and systems.

Dr. York was the recipient of the 1993 Army Research Office Young Investigator Award and the 1996 Office of Naval Research Young Investigator Award.